Available online at www.sciencedirect.com

SCIENCE DIRECT®

Tectonophysics 388 (2004) 253–269

TECTONOPHYSICS

www.elsevier.com/locate/tecto

The northern Walker Lane refraction experiment: Pn arrivals and the northern Sierra Nevada root

John N. Louie[a,*], Weston Thelen[a], Shane B. Smith[a], James B. Scott[a], Matthew Clark[a], Satish Pullammanappallil[b]

[a]*Seismological Laboratory and Department of Geological Sciences and Engineering, University of Nevada, Mackay School of Earth Sciences and Engineering, Reno, NV 89557, USA*

[b]*Optim LLC, Reno, NV, USA*

Received 2 July 2003; received in revised form 6 February 2004; accepted 13 June 2004

Available online 25 August 2004

Abstract

In May 2002, we collected a new crustal refraction profile from Battle Mountain, Nevada across western Nevada, the Reno area, Lake Tahoe, and the northern Sierra Nevada Mountains to Auburn, CA. Mine blasts and earthquakes were recorded by 199 Texan instruments extending across this more than 450-km-long transect. The use of large mine blasts and the ultra-portable Texan recorders kept the field costs of this profile to less than US$10,000. The seismic sources at the eastern end were mining blasts at Barrick's GoldStrike mine. The GoldStrike mine produced several ripple-fired blasts using 8000–44,000 kg of ANFO each, a daily occurrence. First arrivals from the larger GoldStrike blasts are obvious to distances of 300 km in the raw records. First arrivals from a quarry blast west of the survey near Watsonville, CA, located by the Northern California Seismic Network with a magnitude of 2.2, can be picked across the recording array to distances of 600 km. The Watsonville blast provides a western source, nearly reversing the GoldStrike blasts. A small earthquake near Bridgeport, CA. also produced pickable P-wave arrivals across the transect, providing fan-shot data. Arrivals from M5 events in the Mariana and Kuril Islands also appear in the records. This refraction survey observes an unexpectedly deep crustal root under the northern Sierra Nevada range, over 50 km in thickness and possibly centered west of the topographic crest. Pn delays of 4–6 s support this interpretation. At Battle Mountain, Nevada, we observe anomalously thin crust over a limited region perhaps only 150 km wide, with a Moho depth of 19–23 km. Pn crossover distances of less than 80 km support this anomaly, which is surrounded by observations of more normal, 30-km-thick crust. A 10-km-thick and high-velocity lower-crustal "pillow" is an alternative hypothesis, but unlikely due to the lack of volcanics west of Battle Mountain. Large mine and quarry blasts prove very effective crustal refraction sources when recorded with a dense receiver array, even over distances exceeding 600 km. New elastic synthetic seismogram modeling suggests that Pn can be strong as a first arrival, easing the modeling and interpretation of crustal refraction data. Fast eikonal computations of first-arrival time can match pickable Pn arrival times.

Keywords: Seismic refraction; Great Basin; Sierra Nevada; Walker Lane; Synthetic seismogram; Crustal structure

* Corresponding author. Tel.: +1 775 784 4219; fax: +1 775 784 4165.

E-mail addresses: louie@seismo.unr.edu (J.N. Louie), satish@optimsoftware.com (S. Pullammanappallil).

0040-1951/$ - see front matter
doi:10.1016/j.tecto.2004.07.042

1. Introduction

1.1. Objectives

In May 2002, we conducted a low-cost seismic-refraction recording experiment across the northern Sierra Nevada and Walker Lane Belt in eastern California and Nevada (Fig. 1). The purpose of this experiment was to obtain basic information about crustal thickness and velocity over a region that had not yet been extensively characterized. Assessments of both geothermal resources and earthquake hazards require at least a general understanding of crustal properties. The commencement of new research programs in northern Nevada on both topics (Concha-Dimas et al., 2002; Louie, 2002; Pancha et al., 2002; Thelen et al., 2002) motivated us to try to add to the data available, which were summarized by Braile et al., 1989.

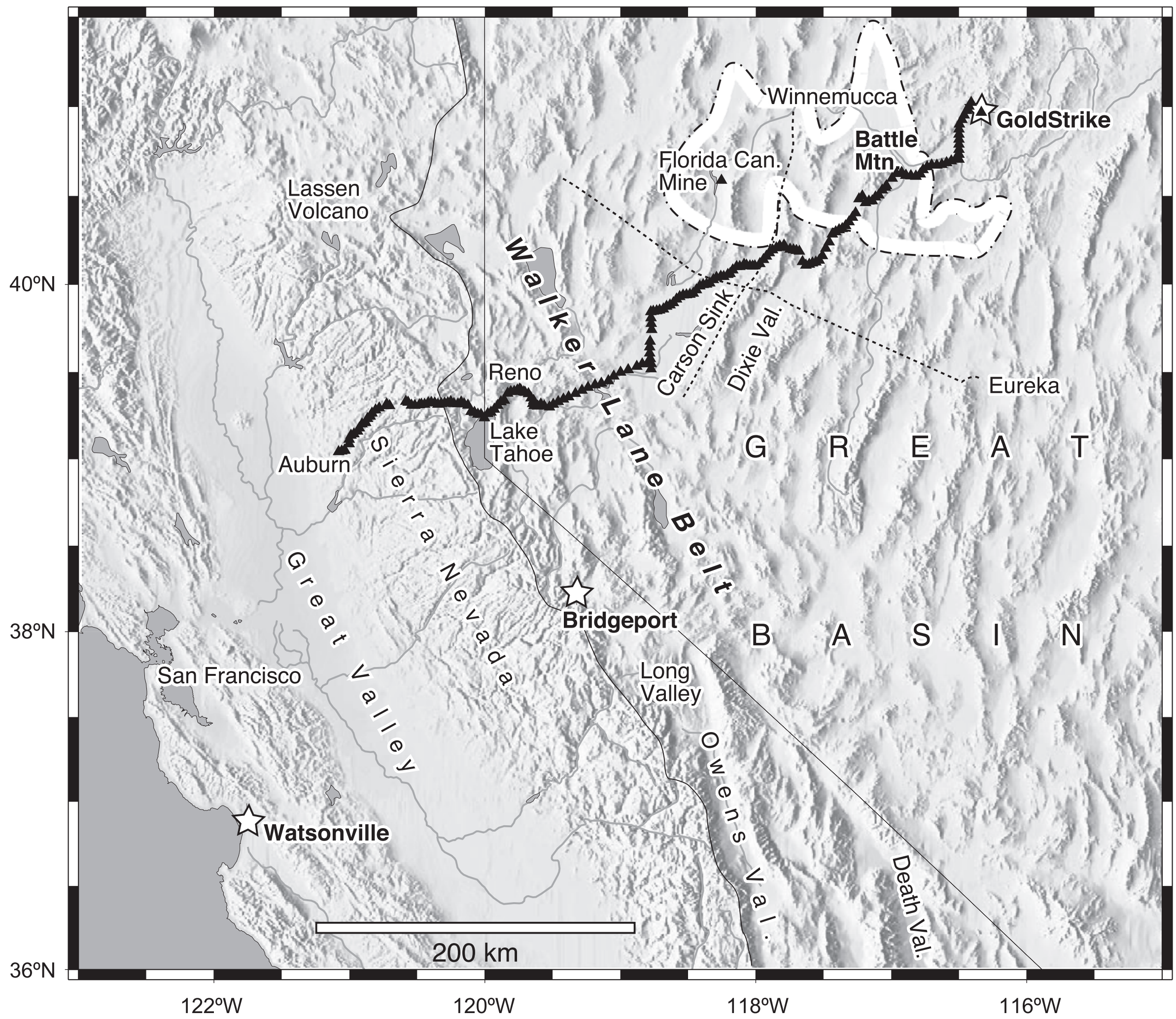

Fig. 1. Map of portions of northern California and Nevada showing receiver locations (path of triangles) and sources (stars) for the northern Walker Lane experiment. The 1986 PASSCAL arrays reported by Catchings and Mooney (1991) are shown with dotted lines. Mapped with GMT (Wessel and Smith, 1991). The thin line along the Sierra crest defines the western limit of the Great Basin physiographic province. The dot–dashed line surrounds the only large region of western Nevada lacking any igneous or volcanic rocks younger than 43 Ma (Stewart and Carlson, 1977).

Because the new research programs had limited funds for gathering new data, we also sought to test the utility of large quarry blasts for long-range refraction surveys. In areas where little detailed information is available, the use of ongoing mining blasts instead of costly drilling and shooting campaigns would substantially reduce the cost of reconnaissance surveys. For quarry blasts to be useful over very long distances they must produce a refracted seismic phase, such as Pn, that is visible above the noise.

If the refracted first arrival is strong enough to be picked, interpretations can use fast, nonlinear Monte Carlo optimizations and inversions (e.g., Pullammanappallil and Louie, 1994; Asad et al., 1999; Lecomte et al., 2000) based on finite-difference eikonal forward-modeling of travel times (Gray, 1986; Vidale, 1988; Podvin and Lecompte, 1991; Qin et al., 1992; Hole and Zelt, 1995) instead of those based on raytracing inversions for secondary phase times (Roecker, 1982; Um and Thurber, 1987; Zelt and Ellis, 1989; Phillips, 1990). For reconnaissance surveys having few sources, it is particularly important to use an optimization and not an inversion, due to the poor formal constraints on the crustal velocity model. Optimizations will produce reasonable models in areas where an inversion would have to be severely overdamped or smoothed (Pullammanappallil and Louie, 1994; Asad et al., 1999). Many workers have noted the difficulty of observing the actual refracted first arrival, whose time is predicted by the fast eikonal computations. Pakiser and Brune (1980) and Jones et al. (1994) examined this issue for the southern Sierra Nevada root; Okaya et al. (2002) discussed Pn for the New Zealand Southern Alps root.

1.2. Previous Work

The objective of this work was seismic reconnaissance of the Walker Lane as a crustal boundary. The Walker Lane Belt (Fig. 1) is a system of fault structures east of the Sierra Nevada that may carry up to a quarter of the Pacific–North America relative plate motion, 12–15 mm/year of dextral strike-slip in total (Faulds et al., 2000; Henry and Perkins, 2001). The Walker Lane extends from the Eastern California Shear Zone at Owens Valley and Death Valley toward the Cascade Range, perhaps as far north as Lassen volcano (Stewart, 1988). Faulds et al. (2000) propose it forms an incipient transform zone, progressively breaking to the northwest. Cashman and Fontaine (2000) divide the Walker lane in the vicinity of Reno into domains consisting of either predominantly northwest-striking right-lateral faulting, or predominantly east–northeast-striking left-lateral faulting. Our refraction profile crosses the northern section of the Walker Lane within the dominantly left-lateral Carson domain.

Our work covers the Walker Lane region between the 1986 PASSCAL experiment in northwest and central Nevada interpreted by Catchings and Mooney (1991), and northern Sierra foothills studies by Spieth et al. (1981) near Auburn, CA. The wide-ranging experiments of Eaton (1963) and Pakiser and Brune (1980) also obtained refraction data from the northern Sierra Nevada, but with widely spaced receivers. Most teleseismic receiver-function analyses nearby were made to the southeast of this profile (Ozalaybey et al., 1997). Crustal thicknesses from the stations on our profile at Battle Mountain and West Humboldt Range (in northeast Carson Sink in Fig. 1) agreed with those of Catchings and Mooney (1991). Braile et al. (1989) reviewed the crustal refraction coverage available. Thelen et al. (2002) assembled the existing crustal velocity data into a comprehensive grid for all of California and the western Great Basin, as part of a regional assessment of the potential for geothermal resources.

Mooney and Weaver (1989) interpreted the existing data to suggest we should find a very shallow, 40-km-deep crustal root below the northern Sierra Nevada, with the crust thinning gradually to 30 km toward Battle Mountain. A relatively shallow root might be expected in the northern Sierra, suggested by the relatively low topographic expression of that part of the range (Fig. 1). For the southern Sierra Nevada, Jones et al. (1994), Wernicke et al. (1996), and Ruppert et al. (1998) have reviewed the evidence for a root as shallow as 33 km, despite the great topography of the High Sierra. Jones et al. (1994) proposed erosion of a heavy eclogitized root (Ducea and Saleeby, 1998) by mantle tectonics into a “drip” of dense material to 100 km depth that produces early teleseismic arrivals. They also discussed possible effects of 3D structure on the Pn arrival, including the possibility that diffracted or “tunneling” Pn at strong lateral contrasts may become invisible in some areas.

The effects of laterally varying crustal structure on the visibility and variations of seismic arrivals such as Pn are highly non-linear. Numerical modeling of elastic wave propagation through such structure greatly aids in understanding effects such as diffraction and tunneling (Larsen et al., 2001). Recently we have developed the ability to compute finite-difference elastic synthetic seismograms up to 1 Hz frequency across hundreds of kilometers of laterally variable terrain. Larsen (2002) has demonstrated the accuracy and accessible cost of long-distance, 3D crustal finite-difference modeling with synthetics for the southern Great Basin. We can now attempt to understand Pn arrivals on closely spaced arrays with full-wave synthetics through complex crustal structure.

2. Methods

We designed our profile to capitalize on an opportunity for very inexpensive crustal refraction surveying. The work of Harder and Keller (2000) at UTEP inspired us; they had used 150 Reftek RT-125 "Texan" instruments to successfully record first arrivals to 150-km distances from a single quarry blast in southern New Mexico. The Texans are far easier to deploy over long (>10 km) profiles than previous generations of independent recorders. One person can easily place or retrieve 30 elements of an array, across 100 km or more, in a single day. The Texans thus minimized the cost of recording.

Like Hawman et al. (1990), and Harder and Keller (2000), we also took advantage of seismic sources that are available for free to accomplish this experiment at a small cost. The Barrick GoldStrike mine, located in northeastern Nevada, has excavated an open pit 3 km in diameter and 0.5 km deep. Once each day, a series of blasts ranging in size from 20,000 to 100,000 lb (8–45 tons) of ANFO gel explosive are set off in rapid succession. The remainder of the workday is devoted to removal of the broken rock, and drilling and loading the next day's blast holes.

With the kind advice and cooperation of Barrick, we anchored the northeast end of our experiment at their GoldStrike mine in northern Nevada. Aiming along routes of easier road access to plant the recorders, and crossing the Walker Lane almost at a right angle, we set the southwest end of the profile near Auburn, CA (Fig. 1). This profile follows a structural and geothermal-resource trend known as the Humboldt lineament (Blewitt et al., 2002).

We deployed on May 20, 2002 and set the Texans to record during mine working hours only on May 21 and 22. Retrieval was completed May 23. The field crew was instructed to set recorder locations along the survey corridor at a fixed interval of about 2.5 min of longitude (except for places where the survey trended north for several stations). The resulting station spacing averaged 4.5 km. Handheld GPS gave station coordinates to 10 m accuracy and elevations to 30 m.

The 199 Reftek RT-125 recorders were linked to 4.5-Hz single geophones, with the entire instrument buried 0.5 m below the ground surface for temperature stability. Few of the instruments logged a total clock drift of more than 30 ms over the 3.5 days between GPS synchronizations. We set the recording schedule to obtain a 235-s record, wait the 5-s minimum between records, and then record another 235 s of data. The sample rate was 200 Hz. Location error and clock drift together should contribute less than 50 ms timing error.

To obtain blast times, we placed recorders on GoldStrike as well as Florida Canyon mine property (Fig. 1), within 2 km of the expected blasts. On both May 21 and 22, we videotaped the GoldStrike blasts from an overlook across the pit, while reading the seconds from a GPS clock into the video's soundtrack. Absolute timing of video observations should be accurate to 0.5 s. The May 21 video shows three shots, all 40,000 lb (18 tons) or less. The May 21 arrivals were recorded, picked, and checked for consistency, but are not reported here.

The May 22 video also shows three shots separated by about 10 s: 20,000 lb (8 tons); 40,000 lb (18 tons); and at 21:15:57 UTC, 100,000 lb (45 tons) of ANFO gel in 100 holes 30 m long each. Figs. 2a and b shows the record of these blasts across the entire array of 199 recorders, plotted with variable-density and wiggle-trace amplitude representations, respectively. The first arrival from the 100,000-lb blast is obvious to at least 300 km distance. The video does not suggest any delay of more than 0.5 s across the array of shot holes. Plumes of rock from the holes blew more than 30 m into the air. The 40,000-lb shot, 10 s earlier, created similar plumes and also appears in the record of Fig. 2a. The 20,000-lb shot, the first on May 22, does not appear on the video to have generated plumes but to have detached a mine bench from the pit wall. This smallest shot is not clearly visible in Fig. 2a or b.

We originally hoped to record a reverse shot from one of several aggregate quarries in the western Sierra near Auburn, CA. The USGS Northern California Seismic Network did not, however, detect any nearby quarry blasts during the days we were recording (D. Oppenheimer, personal communication 2002). That network does have high-gain stations in the western Sierra.

Instead, by sheer luck we recorded a large quarry blast near Watsonville, CA. on May 21. Although south of the survey line direction and more than 240 km from our nearest recorder at Auburn (Fig. 1), this blast provides an approximate reversal. The event was rated at local magnitude 2.2 by the seismic network, with an origin time of 21:28:10 UTC. The timing should be relatively accurate, since network station coverage is very dense in the Watsonville area, since it is on the San Andreas fault.

We also were able to pick arrivals from a magnitude 1.6 earthquake on May 22 at 22:00:49 UTC, near Bridgeport, CA (Fig. 1). The Northern Nevada Seismic Network observed this event on 14 stations and placed it at 2–8 km depth. This earthquake provides a fan shot from the south. At least a dozen more regional earthquakes appear in the records, as do two magnitude-5 teleseisms from the Kuril and Mariana Islands on May 21. Since we recorded only during working hours, to extend the deployment period but stay within the Texans' 64 Mb of memory, we missed at least one magnitude 4 California earthquake during the night of May 21 that would have made a better reversal.

The records from the Texan recorders were converted to SEG-Y format without time adjustment, although clock drifts were checked. Simultaneous 235-s traces from the 199 Texans were concatenated into record sections. From that point, geometry application, processing, display, and picking could be completed entirely within the open-source JRG seismic processing system (http://www.seismo.unr.edu/jrg).

Generation of a 2D velocity model from our recording of the GoldStrike shot and the approximate reversal from Watsonville, across a crooked line of stations (Fig. 1), required a 2D geometry reduction. We aligned stations into a 2D section according to their actual distance from GoldStrike. For time picks from the Watsonville blast, the time was translated into a delay by subtracting a model P arrival time (with 6.0 km/s crust overlying 7.8 km/s Moho at 35 km depth) for the actual receiver distance from Watsonville, and then adding the delay to a model time computed with the station's distance from GoldStrike. This 2D reduction should allow near-surface anomalies to invert in place. Differences in distances used for computing model times ranged from zero at Auburn to a maximum of 56 km near GoldStrike, averaging 41 km. Deeper velocity boundaries could be laterally smeared over such distances in our results.

We estimate a 2D velocity model from the forward and reverse 2D times using the first-arrival time optimization of Pullammanappallil and Louie (1994). This procedure applies Monte Carlo forward time computations (similar to Vidale's, 1988 fast eikonal first-arrival method) with random model changes accepted according to a simulated annealing criterion. Optim's SeisOpt®@2D™ software was used. The optimization is more effective than linear inversions in producing reasonable models where few constraints are available (e.g., Asad et al., 1999). No a priori constraint on the interval between Watsonville and Auburn needed to be specified, even though no picks are available in that region. Further, since the optimization produces the closest travel-time fits when it is least constrained, P velocities are allowed to range from 0.1 to 20 km/s, and anomalies up to 100 km depth are tried. The velocity models created by this optimization are somewhat smoothed and do not intrinsically define the locations of discontinuities such as the Moho. The optimization does not use any reflection times or any amplitude information.

The scalar-wave finite-difference technique of Vidale et al. (1985) generated the acoustic synthetic seismograms we used to examine the properties of the Pn arrival. Elastic finite-difference synthetics employed the methods of Larsen and Grieger (1998) and Larsen et al. (2001). Both of these codes were used in their two-dimensional modes.

3. Results

3.1. Survey procedure

Comparison of video observations of various GoldStrike blasts against the record sections of Fig. 2a and b suggests that much of the blasting activity in current Carlin-trend mining practice can produce excellent crustal refraction data, with obvious first arrivals to at least 250 km distance. Hawman et al. (1990) report getting similar blast data during the 1986 PASSCAL experiment, the last time densely spaced receivers were set out across this region. Very large blasts are conducted in several mines in the area at least once a week, and any ripple-firing delays introduced by the shooters are insignificant compared to the long travel times we are measuring.

Fig. 3 plots our time picks from the GoldStrike and Watsonville blasts and the Bridgeport earthquake as filled symbols, against a longitude axis, not distance. The open symbols are times predicted by the simple, uniform crustal model used above for the 2D

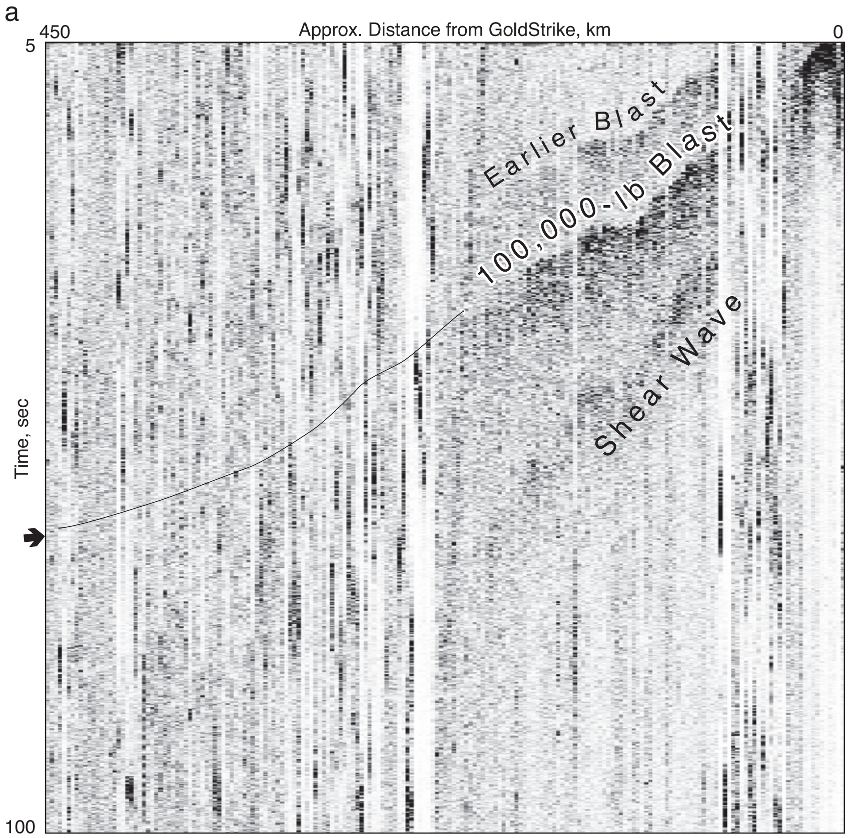

Fig. 2. (a) Example record showing the largest May 22, 2002 blast at Barrick's GoldStrike mine recorded on the 450-km-long array of 199 Reftek RT-125 "Texan" recorders. The traces are arranged in order of recorder longitude, not distance, so some undulations in arrival times are due to crooked-line geometry. For this display the record was low-pass filtered (with a 20% taper filter in the frequency domain at 10 Hz) and plotted with low amplitudes white and larger amplitudes darker, positive or negative. The first arrival from the ~100,000-lb (45 ton) blast is obvious to at least 300 km distance; the arrow shows the arrival time at Auburn (Fig. 1), and the thin line is a few seconds in front of the picks at the larger distances. (b) Alternative wiggle-trace display of the largest Barrick GoldStrike blast on May 22, 2002, not low-pass filtered. Trace-amplitude equalization has been applied. The horizontal axis is true source–receiver distance, with the minimum distance and the GoldStrike mine on the right. The time axis is reduced at 7.4 km/s. The gray line shows where we made the first-arrival picks in Fig. 3, thickening with distance as our uncertainty in arrival time grows from 0.1 to 1.5 s. The Pn arrival between 80 and 280 km distance truncates shingled PmP reflections, sloping up and to the left in this plot, arriving from parts of the Moho having different depths and dips.

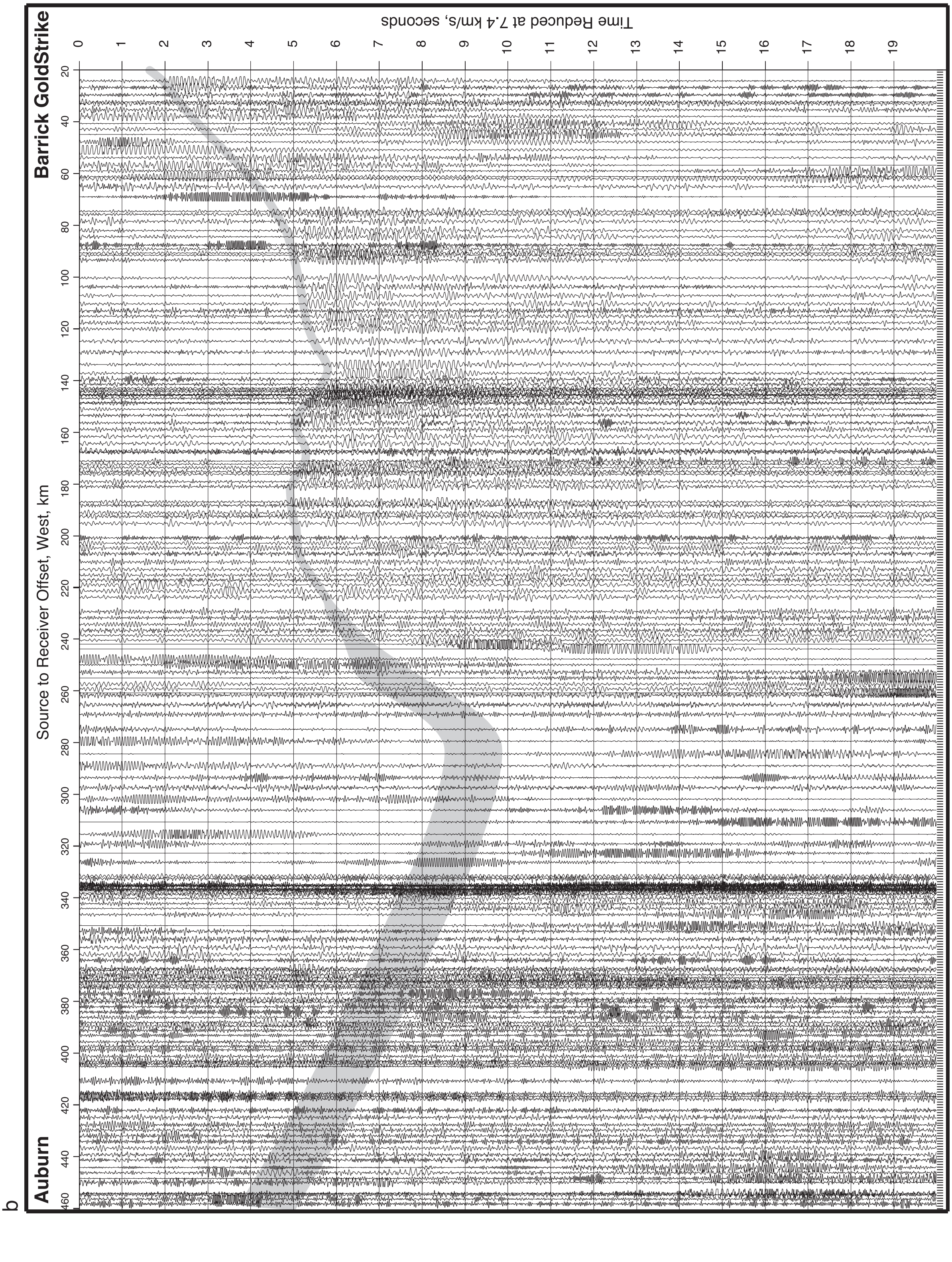

Fig. 2 (continued).

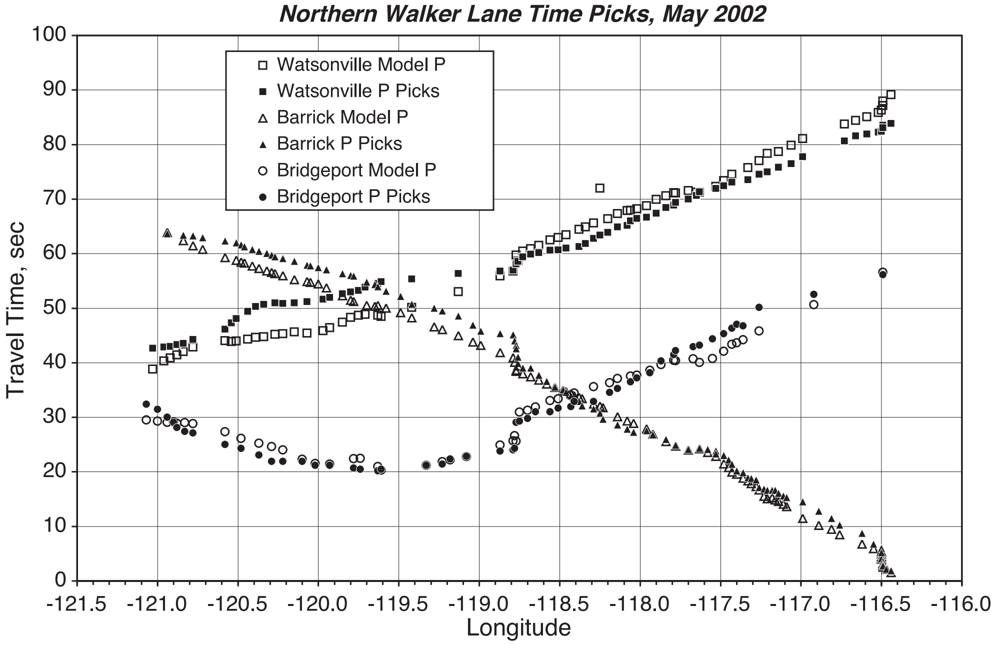

Fig. 3. Time picks across the recording array, arranged by longitude, from three sources: the May 22, 2002 GoldStrike blast, a large blast the previous day at a quarry near Watsonville, CA, and a small earthquake on May 22, 2002 near Bridgeport, CA. The model P arrival times were computed for a uniform 6.0 km/s crust overlying a 7.8 km/s Moho at 35 km depth. Since 3D geometry has been projected onto a 2D profile, preserving true distances, plotting times by station longitude makes the consistent receiver delays visible.

geometry reduction. Picks are sparser in the noisy areas where we placed the receivers near busy highways. The noisy intervals are clear in Fig. 2 as well, with a section of Interstate 80 near GoldStrike, and a section in the center of the array along US Highways 95 and 50 in the Carson Sink. The noisy sections do not predominate, and so our procedures achieved a long-distance record at very low cost.

Given the small 50-ms maximum instrumental and location timing error, the variations of pick times seen in Fig. 3 probably form a more fair summary of the errors in the data fed to the velocity optimization. Mis-picked phases and the crooked receiver-line geometry may contribute 1 s of uncertainty to the times. Since we are modeling 3D picked times with 2D velocity models, such variations will represent inconsistent data.

3.2. Delay times

Examining the GoldStrike and Watsonville picks in Fig. 3 for the most prominent delay features relative to a uniform crust, two observations are clear. First, between $-119°$ and $-117.5°$ longitude, Walker Lane to Dixie Valley, Nevada (Fig. 1), the picks are advanced relative to the model, more so from Watsonville. This observation suggests thin crust east of the Walker Lane. Second, from the Walker Lane west across the northern Sierra, the GoldStrike and Watsonville picks are all delayed by 4 to 6 s. Note that the delay reduces significantly at Auburn. A simple explanation of these picks, if they truly represent first-arrival times, would be a thick crustal root under the northern Sierra Nevada.

The north-traveling fan arrivals from the Bridgeport earthquake only partially support this result. The fan arrivals are similarly early just east of the Walker Lane, adding support to the model of a shallow crust in the Carson Sink–Dixie Valley area. As well, the Walker Lane is clearly a significant boundary in crustal thickness, perhaps less than 100 km in width. However, fan arrivals in the Sierra Nevada are a few seconds early, not delayed. Pakiser and Brune (1980) also observed fast Pn propagation along the trend of the Sierran root. Jones et al. (1994) explained such a discrepancy in the southern Sierra Nevada as a 3D effect, with longitudinally propagating Pn traveling obliquely along the steep walls of the root. For the Bridgeport fan picks to be explained this way, the root must be narrow, with the potential for fan-shot Pn to "tunnel" across the root, or to jump from one high-velocity side of the root to the other. Longitudinal first arrivals would never propagate down the deep center of the root in such a model.

3.3. Prior model

Thelen et al. (2002) assembled prior-model information from the review papers by Braile et al. (1989), Mooney and Weaver (1989), and Thompson et al. (1990). The velocity profiles closest to our profile were placed on our 2D section, and linear interpolations made between them. The interpolations do not necessarily preserve sharp discontinuities across the section between profiles that have a discontinuity at different depths. Fig. 4 shows the result, with a 30-km-deep Moho east of the Walker Lane deepening rapidly west into a small 42-km-deep Sierran crustal root. The prior model's root would be centered under Reno and Lake Tahoe, near the topographic crest of the range.

3.4. Optimized velocity model

We applied the velocity-model optimization of Pullammanappallil and Louie (1994) to our 2D time picks from the GoldStrike and Watsonville blasts. There are no sources near the center of the profile. Fig. 5 compares the picks (symbols) against the first-arrival times predicted by the optimized model (thick lines) on a reduced-time axis. In Fig. 5, the times from GoldStrike are black and the times from Watsonville are gray. Eikonal (Vidale, 1988) first-arrival times through the optimized model match the picks well, with a mean-squared error of 0.62 s^2. The predicted times are mostly within 1 s of the picked times; all predictions are within 2 s. The picks most inconsistent with a 2D model, from the most crooked parts of the array, are fit the most poorly.

Fig. 6 presents the contoured optimized velocity-model section. The optimization result is an average of a large number of trial models that fit the picks equally well. It produces the travel-time fits (thick lines) in Fig. 5. The optimization result is presented only as far west as Auburn, and not all the way to Watsonville. With the Watsonville shot 240 km from Auburn, the Sierra Foothills end of the model is least well constrained, especially in the upper crust. We have thinned the contour lines we believe are least reliable. The limit of constraint is placed where the model's ray coverage drops to zero. On the west side of the model, most rays will be nearly horizontal. The ramp in the limit of constraint down to the west reflects how the optimization has placed an 8.0 km/s Pn refractor under the Great Valley at 50 km depth.

The low velocities near the surface west of the Walker Lane (A in Fig. 6) are likely the result of the

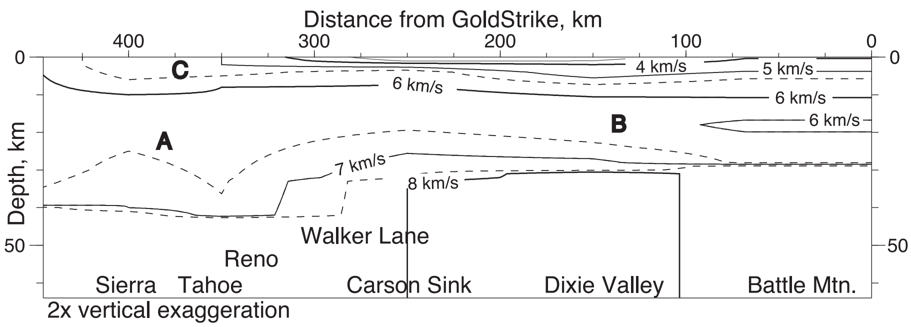

Fig. 4. Contour plot of the "prior model" for crustal structures interpreted by previous workers near the location of our refraction survey. Solid contours are marked at 1 km/s intervals. Dashed contours are drawn between 5.5 and 7.5 km/s to show better the velocity patterns at depth. The model is a compilation of 8 different refraction and receiver function studies listed in the text. These studies assume the Moho is reached at velocities between 7.5 and 7.8 km/s. Note the presence of a muted crustal root under the Sierra Nevada near (A). Considerably thinner crust is present east toward (B). The lack of low velocities at the surface in the Sierra Nevada at (C) is due to a lack of resolution at the surface in previous studies. Contoured with GMT (Wessel and Smith, 1991).

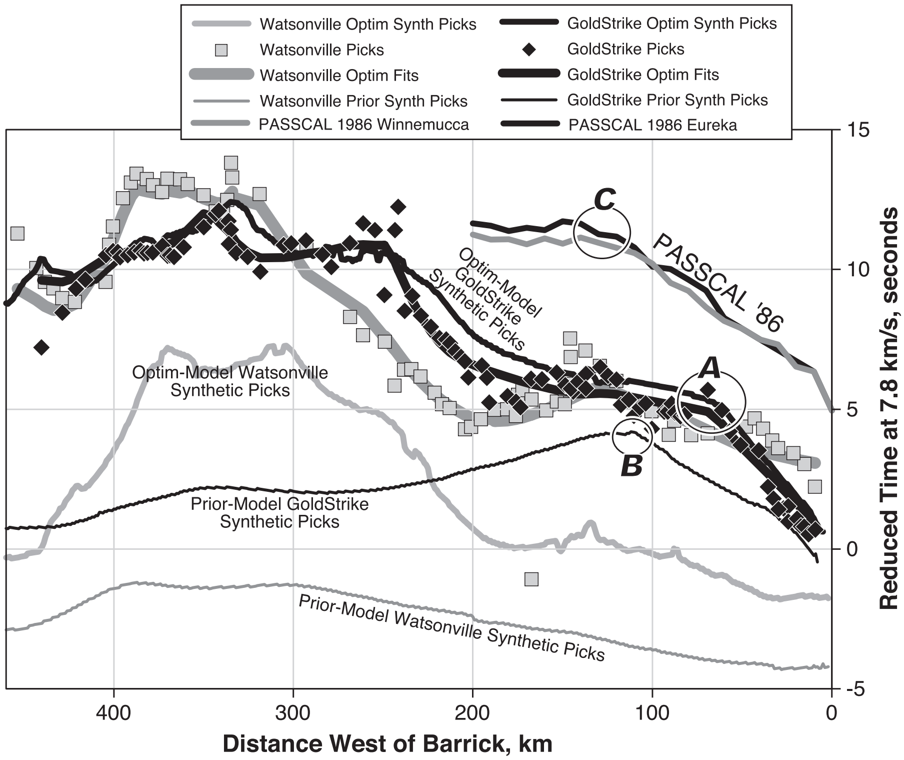

Fig. 5. GoldStrike (black) and Watsonville (gray) blast picks plotted as times reduced by 7.8 km/s according to a 2D distance calculation. Included are picks from 2D elastic synthetics generated from prior and optimized models. Times picked from the Winnemucca and Eureka blast data from the 1986 PASSCAL arrays reported by Catchings and Mooney (1991) are plotted after adding 5 s for clarity. The Pn crossovers are labeled A, B, and C for discussion in the text. While crossover (A) for our survey is near Battle Mountain (Fig. 1), the crossovers (C) are reached by the 1986 PASSCAL lines 100 km to the southwest, between Carson Sink and Dixie Valley (Fig. 1).

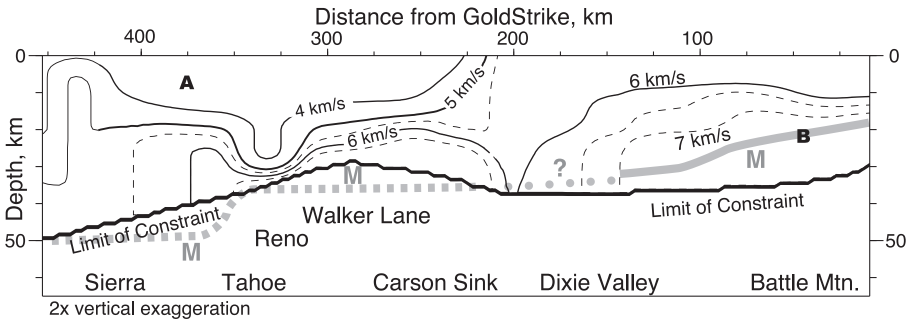

Fig. 6. Contour plot of the optimization of our refraction results along the same section as the “prior model” of Fig. 4. Contours and scales have remained the same. The thick gray line and the “M”s trace our interpretation of Moho depths. The most striking differences between our model and the prior model are seen at (A) and (B). Below (A), a prominent root is present under the Sierra Nevada. Here, lower-velocity crust is found at least 10 km deeper than previously imaged. We infer that strong velocity–depth gradients in the lower crust keep our deepest diving rays and the lower limit of constraint above the Moho (broken gray line), in velocities <7 km/s. At (B), we find much thinner crust than previous workers had indicated, from 5–10 km thinner, depending upon the source. The thick gray line traces the upper limit of 7.4–7.6 km/s velocities; higher velocities are not consistently seen above the limit of constraint. The horizontal ray set between Carson Sink and Dixie Valley does not find the Moho in that interval (gray dotted line and “?”; where Catchings and Mooney, 1991, imaged the Moho at this depth). Results on the west end past 425 km distance should be ignored due to the lack of time picks past 450 km. Contoured with GMT (Wessel and Smith, 1991).

4–6 s of delay observed there (Figs. 3 and 5). The low velocities are not further constrained by any sources in that region. We made a trial optimization run for which velocities were constrained to the range 5.0–8.5 km/s. This run could fit the travel times without the low velocities in the Sierran upper crust, but only with twice the error of the preferred model, at 1.23 s^2. To try to match the delays, the resulting model (not shown) pushes velocities below 6 km/s to more than 60 km depth under the western Sierra, and more than 50 km depth under Reno.

This velocity-constrained model does retain the very thin crust below Battle Mountain, found by our preferred model. It also produces reasonable variations in Pg velocities between the felsic Sierra Nevada, at 5.0–5.5 km/s, and the more mafic Great Basin, at 6.0–6.5 km/s. In this trial model as well, velocities above 7.4 km/s are needed in just a few places to turn the mostly horizontal ray set.

The largely horizontal ray set and lack of sources within the array has led to a discontinuous picture of the Moho. The optimization only places a velocity gradient like a Moho refractor where it is needed to turn rays. Thus, the apparent deepening of the Moho at Dixie Valley probably represents instead a gap in evidence for a Pn refractor. At this location, between 150 and 200 km distance in Figs. 4 and 6, Catchings and Mooney (1991) and Holbrook et al. (1991) have excellent evidence of a 7.8 km/s Moho at 30 km depth (shown in Fig. 4). The optimization is similarly parsimonious in setting velocities high; few areas of the section in Fig. 6 exceed 7.2 km/s. Higher velocities at the Moho are not needed to fit the time picks.

Under the western Sierra at Auburn, though, the downward ramp in the limit of constraint (Fig. 6) represents the eastern limb of the deepest-diving rays in the preferred model. These rays turn at 52 km depth below the Great Valley, and appear to cut across a steep-walled Sierran crustal root without turning within it. The root appears to extend from the eastern edge of the Great Valley to Lake Tahoe, a width of 100 km or less. Fig. 6 shows the eastern half of the root.

The northern Sierra Nevada crustal root appears at least 50 km deep, with a steep wall bounding it just west of Lake Tahoe, at the topographic crest of the range. There is no evidence for velocity stratification within the root; values of 5.5–6.0 km/s continue to the base of constraint. Our results do not constrain where the deepest center of the root may lie, except that the entire root lies west of Lake Tahoe and the topographic crest.

The model suggests that the Pn rays from Watsonville may be tunneling across a deep, narrow root, as Jones et al. (1994) suggested. With no receivers west of Auburn (Fig. 1), upper-crustal velocities are not constrained at the western edge of the section in Fig. 6. However, the Pn rays passing below from the Watsonville blast do constrain deep-crustal velocities, since they emerge over the areas we have receivers, 100 km farther east in the Walker Lane. The apparent tunneling of these rays across the root is additional evidence the root is deeper than 50 km, and steep-sided.

A striking feature of our optimized model is the very thin crust placed under Battle Mountain (B in Fig. 6). The depth to velocities of 7.2 km/s is as little as 19 km at the east end of the model. Where the optimized velocities get as high as 7.5 km/s, they occur in that region as shallow as 21–23 km depth. Crustal thicknesses below the Walker Lane are more in concord with the prior model (Fig. 4), with velocities of 7.8 km/s being reached at 32–35 km depth. On the other hand, the deep zone of low crustal velocities below Reno may be a result of poor constraint, from the largely horizontal rays coming from Watsonville.

We ran additional trial optimizations using a fixed 1D crustal structure, and others with a fixed Moho having a fixed velocity. None of these trial constrained optimizations could achieve a mean-squared misfit of less than 1.79 s^2, almost three times the misfit of the preferred result of the freely varying optimization at 0.62 s^2. Fixing crustal velocities to 19 km depth resulted in a 19-km-deep Moho across the entire half of the section east of the Walker Lane, and a 50-km-deep Sierran root, with 3.12 s^2 misfit. Fixing a 7.8 km/s Moho at 34 km depth produced the 1.79 s^2 misfit, but forced wildly unrealistic crustal velocities reaching 7.0 km/s at 10 km below Battle Mountain, and at 2.0 km/s 10 km below the Sierra crest. The result of this trial suggests that our preferred model (Fig. 6) has made a reasonable balance between lateral velocity variations in the crust, and Moho topography.

It is certainly possible that the low upper-crustal velocities in Fig. 6 partly result from 3D effects uncontrolled by our off-line Watsonville reversal. Within the limits of the 2D reduction, it appears that constraining crustal velocities to a more reasonable 5.0 km/s minimum doubles misfit and demands a Sierran root that is both deep and very wide. The fixed-Moho tests show that substantial Moho topography is needed for a reasonable fit. Yet our preferred model is relatively parsimonious about projecting Moho topography from the time delays. There is no way to fit our data set with simultaneously less radical velocities and Moho topography.

3.5. Synthetic seismograms

To generate synthetic seismograms from our preferred optimized velocity model of Fig. 6, we had to extend velocity values beyond the depth of constraint. We did this by simply pasting the constrained part of the optimized model within our prior model of Fig. 4. This compositing created some velocity contrasts that probably do not exist, such as an 8.3 km/s Moho below Dixie Valley and an 8.0 km/s Moho below the Sierran root. Between Auburn and Watsonville (Fig. 1) the prior-model crust is faster and thinner than it is in the unconstrained western part of the preferred model.

We generated both 2D acoustic and elastic synthetic seismograms across both the prior and optimized velocity models, from sources at Watsonville and GoldStrike. Fig. 7 shows the acoustic and elastic synthetics across the optimized model from the GoldStrike source. All the acoustic synthetic sections show a weak first-arrival Pn diffracted by the edges of the Sierra Nevada crustal root. A secondary phase one to three orders of magnitude stronger follows the weak acoustic first arrival by 6–10 s. The acoustic synthetics suggest that, in the presence of noise, attempts to pick the first arrival would always pick the secondary arrival instead, giving a late pick time and a falsely thick crust.

The new elastic synthetics for our models completely counter the above "general wisdom" gained from experience with acoustic and kinematic modeling. The fully elastodynamic methods (Larsen et al., 2001; Larsen, 2002) generate synthetic seismograms that have consistently strong Pn first arrivals, as the lower panel of Fig. 7 shows. We observed weak acoustic, countered by strong elastic Pn arrivals with all four combinations we computed of prior and optimized models and GoldStrike and Watsonville sources. Fig. 7 makes it clear that, if any arrivals can be picked through the noise at those distances, the true Pn first arrival can be picked. There is not a stronger secondary phase. The acoustic equations may turn too much energy downward. With the elastic equations local P-to-S conversion at the edge of the root followed by immediate conversion back to P at the next finite-difference grid point could reinforce the amplitude of the diffracted Pn.

The elastic synthetics, bottom of Fig. 7, show an overall reduction in amplitude at the edge of the steep-walled Sierran root. The GoldStrike data in Fig. 2a and b show a similar reduction, although it starts further to the east. Pn clearly rolls off into a weaker diffraction, radiating from the corner where the Moho suddenly deepens. This rolloff is also a feature of the Watsonville elastic synthetics (not shown), but the Watsonville data are too far to the east to observe the strong arrivals west of a diffraction from a Moho corner at the east edge of the Great Valley. Jones et al. (1994) observed a similar rolloff across the southern Sierra, but only when seismic waves were propagating from the west. The steepness of the east wall of the root must be lesser in the south than in the northern Sierra.

Fig. 2a and b also show a short segment of amplitude increase at 340 km distance from GoldStrike, mimicked by the elastic synthetic. This increase appears to be due to focusing by the low-velocity anomaly below Reno at 30-km depth (Fig. 6). Although the deep low velocities may not be reasonable, whatever causes the delays also must cause amplitude focusing.

Fig. 5 shows picks from the elastic synthetics in reduced time against the data picks, as thin lines. The synthetic picks from the GoldStrike source through the optimized model are seldom more than 1 s later than the data picks. The Watsonville synthetic picks through the optimized model are 4–5 s early, because of the mismatch between the models in the unconstrained region between Watsonville and Auburn. The synthetic and data picks show

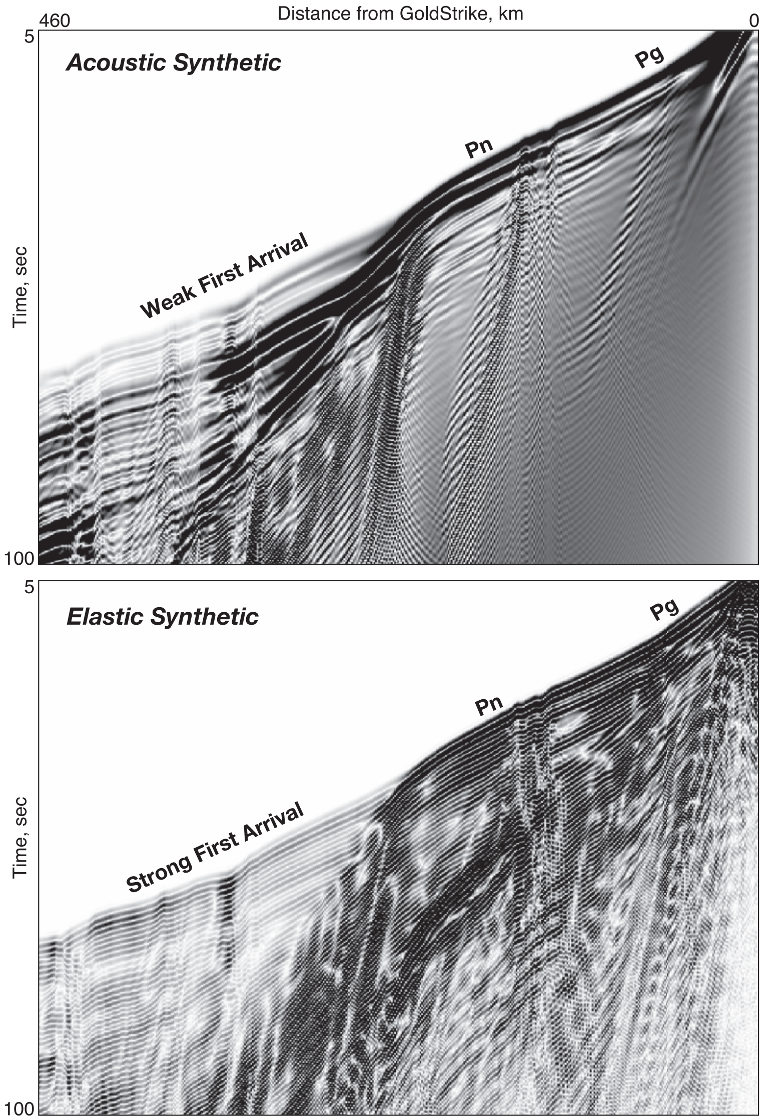

Fig. 7. Acoustic and elastic finite-difference synthetic 2D record sections to 460 km distance, computed from the optimized velocity model of Fig. 6 for the GoldStrike blast. Compare these plots to Fig. 2a. Larger positive and negative amplitudes are darker, after the application of trace equalization. The acoustic synthetics suggest much smaller Pn amplitude compared to late phases, beyond the lateral discontinuity at the Walker Lane. The elastic synthetics show instead that the Pn first arrival has significant amplitude and can be picked so long as any arrivals are visible.

very similar delays across the Sierra Nevada, however. For both sources the synthetic picks from the prior model are much earlier than the data picks. The prior model shows less than 3 s delay over its shallow Sierran root, whereas the data and the optimized model show 4–6 s delay over a deep northern Sierra Nevada root.

4. Discussion

Our optimized crustal velocity section in Fig. 6 suggests rather extreme Moho topography below the northern Sierra and the northwestern Great Basin. This is particularly the case with the deep, >50 km, narrow root we suggest for the northern Sierra, and with the very thin, 20 km crust we observe near Battle Mountain. Such extreme topography on the Moho has been documented in a few places. Ruppert et al. (1998) found substantial changes in Moho depth and crustal velocities across the southern Sierra. Lewis et al. (2001) suggest as much as 20° Moho dip from a root under the western side of the California Peninsular Ranges up to very thin, extending crust in the Gulf of California. Our similar observations of a deep root under the western side of the northern Sierra, combined with the thin crust below Battle Mountain, may form an analogue to the Peninsula Ranges features. Blewitt et al. (2002) identify the volcanics-poor region just west of Battle Mountain (outlined in a dot–dashed line in Fig. 1) as having one of the larger rates of extension in the northern Great Basin.

Such thin crust, 20–25 km, has only been seen elsewhere in the Great Basin in Utah at the transition to the Colorado Plateau, by refraction experiments (Keller et al., 1975). Receiver–function inversions constrained by 25-s surface-wave phase velocities by Ozalaybey et al. (1997) at Battle Mountain have a sharp Moho at a deeper 28 km depth, but only use teleseismic arrivals from the southeast. Their result is conceivably compatible with our 23-km Moho depth there only in the presence of large dips on the Moho just south of Battle Mountain. Battle Mountain did yield their thinnest crust out of all the stations they examined across the Great Basin. The Ozalaybey et al. (1997) results at West Humboldt Range, at Carson Sink in Figs. 1 and 6, show a velocity ramp in the lower crust grading into mantle velocities at 34 km depth, very similar to our optimized model.

Fig. 5 shows why our optimization puts such a thin crust below Battle Mountain. The Pn crossover from GoldStrike at A in Fig. 5 is at only 70 km distance—the observation that led to the modeling of thin crust (Fig. 6). These were the easiest picks to make, obvious in the records of Fig. 2. The assembled prior model with a 30 km crust gives the expected crossover at B in Fig. 5, at 110 km distance. PASSCAL 1986 data from Catchings and Mooney (1991) show the Pn crossover at 120 km (lines raised in Fig. 5 by 5 s), leading to their ~35 km crustal-thickness results.

The 1986 PASSCAL arrays extended both north and south of our survey through Battle Mountain (Fig. 1). One explanation of the discrepancy between our close Pn crossover (A in Fig. 5) and the farther crossover of the 1986 results (C in Fig. 5) is as a 3D effect: shallow crust below Battle Mountain does not extend significantly north or south. The 1986 PASSCAL crossovers occur 100 km geographically removed from our crossover, near Dixie Valley and Carson Sink instead of Battle Mountain (Fig. 1). This may explain our depth mismatch with Ozalaybey et al. (1997) as well. This area of thin crust is the part of a feature known as the "Humboldt Lineament" just west of Battle Mountain that shows a high rate of extension normal to the trends of mapped faults in GPS analyses (Blewitt et al., 2002). The area of high extension rate is only 100 km in diameter. This area also shows a high local maximum temperature of thermal waters.

Holbrook et al. (1991) suggested for the northeast tip of the Carson Sink (Fig. 1), from coincident 1986 PASSCAL refraction and reflection data, that extreme Cenozoic extension could lead to mafic intrusion of the lower crust, creating a 7.4 km/s basal–crustal layer. To explain the close "Pn" crossover we observe below Battle Mountain from GoldStrike blasts (A in Fig. 5), such a basal crust would have to thicken to at least 10 km. Klemperer (1987) did show that COCORP reflection data in this area of high heat flow have strong sequences of lower-crustal reflectivity that begin particularly high in the crust.

This unusually thick and high-velocity lower-crustal "pillow" is an alternative hypothesis to our interpretation of unusually thin crust below Battle Mountain. Such a lower-crustal pillow, 10 km thick with a velocity of 7.2–7.8 km/s, would have to be a result of an extremely high volume of basaltic intrusion and underplating. Yet this 100×100 km region west of Battle Mountain appears on geologic maps as one of very few areas of Nevada lacking any volcanic rocks younger than 43 Ma (e.g., Stewart and Carlson, 1977). With the peculiar lack of surface volcanics (dot–dashed outlined region in Fig. 1), and current high rate of surface extension, we interpret a shallow (20 km) Moho at Battle Mountain, and hypothesize extensional thinning of the lower crust.

Fig. 5 also shows the delay evidence for a deep northern Sierra Nevada crustal root. Times picked from the GoldStrike elastic synthetics are a maximum of 1 s later than the eikonal, first arrival times. The elastic synthetic picks have some distance shift due to the somewhat broad source that has to be imposed on a finite-difference grid. The elastic model had 7.5–8.0 km/s velocities from the prior model (Fig. 4) composited in below the 30–35 km depth of constraint of optimization on the east end of our profile (Fig. 6). Since the elastic and eikonal times match (thick black lines in Fig. 5), this reconnaissance survey with sources only at the ends may not constrain any average sub-Moho velocity well. The "Pn" refraction may reflect a lower velocity just at the Moho, or may even be a lower-crustal refraction, such as the "$7 \cdot \times$" phase of Pakiser and Brune (1980).

Our evidence for a deep northern Sierran root is the 4- to 7-s delays in the left half of Fig. 5, compared to the prior model that has only a 42-km root under Tahoe/Reno, from 2- to 3-s delays. The optimized model (Fig. 6) shows a >50 km root west of Tahoe, 10 km deeper than the 40-km root shown by Mooney and Weaver (1989). Our root appears as a steep-walled trough, centered 50 km further west than Mooney and Weaver's. The deep root may have a constant velocity near 6.0 km/s, perhaps evidence for thick upper-crustal rocks above the eclogitized keel as proposed by Ducea and Saleeby (1998).

A deep northern Sierra root does not match the muted topography of the region. There is little previous constraint on the crust across the northern Sierra. Our profile follows the San Francisco–Fallon profile of Eaton (1963) that gave a shallow 40-km root, but station spacing at the time did not allow trace-to-trace phase correlation. With our stations spaced at 4.5 km, we can be much more confident that we are picking the Pn first arrival. The elastic synthetic seismograms also assure us that the Pn arrival will be strong enough to pick.

Does the northern Sierra retain the eclogite crustal root and mantle keel that Ducea and Saleeby (1998) propose detached from the southern Sierra? Unfortunately, our profile cannot image the deepest part of the root. Further work will record sources in the Sierra, to provide a ray set through the root that is less dominantly horizontal. Quarry blasts, as we can find them in the region, will also allow us to put more constraints on upper-crustal velocities. We will continue to exploit the huge blasts at GoldStrike for broad regional reconnaissance.

5. Conclusions

(1) We observe an unexpectedly deep crustal root under the northern Sierra Nevada range, over 50 km in thickness and centered west of the topographic crest. Pn delays of 4–6 s support this interpretation.

(2) At Battle Mountain, Nevada, we observe anomalously thin crust over a limited region perhaps only 100 km wide, with a Moho depth of 19–23 km. Pn crossover distances of less than 80 km support this anomaly, which is surrounded by observations of more normal, 30-km-thick crust.

(3) Large mine and quarry blasts prove very effective as crustal refraction sources when recorded with a dense receiver array, even at distances exceeding 600 km.

(4) New elastic synthetic seismogram modeling suggests that Pn can be strong as a first arrival, easing the modeling and interpretation of crustal refraction data. Fast eikonal computations of first-arrival time can match pickable Pn arrival times.

Acknowledgments

Funded by cooperative grant DE-FG07-02ID14211 administered by DOE, Idaho Operations Office, INEEL, and grant DE-FG36-02ID14311, managed through the DOE Golden Field Office. Many of the instruments used in the field program were provided by the PASSCAL facility of the Incorporated Research Institutions for Seismology (IRIS) through the PASSCAL Instrument Center at New Mexico Tech. Data collected during this experiment are available through the IRIS Data Management Center at www.iris.edu, assembled dataset report number 02-007. The facilities of the IRIS Consortium are supported by the National Science Foundation under Cooperative Agreement EAR-0004370 and by the Department of Energy National Nuclear Security Administration.

Willie Zamora of NMT/PASSCAL provided crucial assistance deploying the instruments. Thanassis Makris, Tom Rennie, Aline Concha-Dimas, Aasha Pancha, Tiana Rasmussen, and Chris Lopez of UNR deployed and recovered most of the recorders. We are indebted to Gary Baschuk, Keith Bettles, and Larry Radford of the Barrick GoldStrike Mine, and to Bob Thomason and the Florida Canyon Mine for allowing us to access their properties, and for information on blast times, locations, and configurations. David Oppenheimer of the USGS in Menlo Park provided invaluable help searching for California quarry blasts. The California Integrated Seismic Network operations of the USGS, UC Berkeley, Caltech, and UNR provided rapid notification of blasts and earthquakes we used from California. The Northern Nevada Seismic Network operated by UNR provided earthquake information from Nevada. All the seismic networks are sponsored by the USGS as part of the Advanced National Seismic System, and by the States of California and Nevada. Chris Loughner of UNR ran the elastic synthetics on the CCoG facility (http://www.seismo.unr.edu/ccog), which is funded by Optim LLC, the Nevada Applied Research Initiative, and Lawrence Livermore National Laboratory.

Contact louie@seismo.unr.edu for a DVD video showing the GoldStrike blasts. Additional project information is available at http://www.seismo.unr.edu/geothermal.

References

Asad, A.M., Pullammanappallil, S.K., Anooshepoor, A., Louie, J.N., 1999. Inversion of travel-time data for earthquake locations and three-dimensional velocity structure in the Eureka Valley area, eastern California. Bull. Seismol. Soc. Am. 89, 796–810.

Blewitt, G., Coolbaugh, M., Holt, W., Kreemer, C., Davis, J., Bennett, R., 2002. Targeting of potential geothermal resources in the Great Basin from regional relationships between geodetic strain and geological structures. Trans.-Geotherm. Resour. Counc. 26, 523–526.

Braile, L.W., Hinze, W.J., von Frese, R.R.B., Keller, G.R., 1989. Seismic properties of the crust and uppermost mantle of the conterminous United States and adjacent Canada. In: Pakiser, L.C., Mooney, W.D. (Eds.), Geophysical Framework of the Continental United States: Boulder, Colorado, Mem. Geol. Soc. Amer., vol. 172, pp. 655–680.

Cashman, P.H., Fontaine, S.A., 2000. Strain partitioning in the northern Walker Lane, western Nevada and northeastern California. Tectonophysics 326, 111–130.

Catchings, R.D., Mooney, W.D., 1991. Basin and Range crustal and upper mantle structure, northwest to central Nevada. J. Geophys. Res. 96, 6247–6267.

Concha-Dimas, Aline, Rasmussen, Tiana, Louie, John N., Smith, Shane, Thelen, Wes, 2002. Las Vegas basin seismic response project: developing a community velocity model for NTS and Las Vegas. EOS Trans. Am. Geophys. Union 83 (Suppl. 47), F1055. (19 Nov.).

Ducea, Mihai N., Saleeby, Jason B., 1998. The age and origin of a thick mafic–ultramafic keel from beneath the Sierra Nevada batholith. Contrib. Mineral. Petrol. 133, 169–185.

Eaton, J.P., 1963. Crustal structure from San Francisco, California, to Eureka, Nevada, from seismic refraction measurements. J. Geophys. Res. 68, 5789–5806.

Faulds, J.E., Henry, C.D., Garside, L.J., Cashman, P.H., 2000. Kinematics of the northern Walker Lane, western Nevada: in pursuit of constraints. Abstr. Programs-Geol. Soc. Am. 32 (7), 106.

Gray, S.H., 1986. Efficient traveltime calculations for Kirchhoff migration (short note). Geophysics 51, 1685–1688.

Harder, S., Keller, G.R., 2000. Crustal Structure Determined from a new Wide-Angle Seismic Profile in Southwestern New Mexico: Guidebook, 51st Field Conf., Southwest Passage—A Trip Through the Phanerozoic. New Mexico Geol. Soc., Socorro, pp. 75–78.

Hawman, R., Colburn, R., Walker, J.D., Smithson, S., 1990. Processing and inversion of refraction and wide-angle reflection data from the 1986 Nevada PASSCAL experiment. J. Geophys. Res. 95, 4657–4692.

Henry, C.D., Perkins, M.E., 2001. Sierra Nevada—Basin and Range transition near Reno, Nevada; Two stage development at ~12 and 3 Ma. Geology 29, 719–722.

Holbrook, W.S., Catchings, R.D., Jarchow, C.M., 1991. Origin of deep crustal reflections: implications of coincident seismic refraction and reflection data in Nevada. Geology 19, 175–179.

Hole, J.A., Zelt, B.C., 1995. 3-D finite-difference reflection traveltimes. Geophys. J. Int. 121, 427–434.

Jones, C.H., Kanamori, H., Roecker, S.W., 1994. Missing roots and mantle “drips”: regional Pn and teleseismic arrival times in the Southern Sierra Nevada and vicinity, California. J. Geophys. Res. 99 (B3), 4567–4601.

Keller, G.R., Smith, R.B., Braile, L.W., 1975. Crustal structure along the Great Basin–Colorado Plateau transition from seismic refraction studies. J. Geophys. Res. 80, 1093–1097.

Klemperer, S., 1987. A relation between continental heat flow and the seismic reflectivity of the lower crust. J. Geophys. 61, 1–11.

Larsen, S.C., 2002. Las Vegas basin seismic response project: 3-d finite-difference ground motion simulations. EOS Trans. Am. Geophys. Union 83 (Suppl. 47), F1054. (19 Nov.).

Larsen, S., Grieger, J., 1998. Elastic modeling initiative: Part III. 3-D computational modeling. Soc. Explor. Geophys. Ann. Internat. Mtg., 1803–1806. (Expanded Abstract).

Larsen, S., Wiley, R., Roberts, P., House, L., 2001. Next-generation numerical modeling: incorporating elasticity, anisotropy and attenuation. Soc. Explor. Geophys. Ann. Internat. Mtg., 1218–1221. (Expanded Abstract).

Lecomte, I., Gjoystdal, H., Dahle, A., Pedersen, O.C., 2000. Improving modelling and inversion in refraction seismics with a first-order Eikonal solver. Geophys. Prospect. 48, 437–454.

Lewis, J., Day, S., Magistrale, H., Castro, R., Astiz, L., Rebollar, C., Eakins, J., Vernon, F., Brune, J., 2001. Crustal thickness of the Peninsular Ranges and Gulf extensional province in the Californias. J. Geophys. Res. 106, 13599–13611.

Louie, John N., 2002. Assembly of a crustal seismic velocity database for the western Great Basin. Presented at the Geothermal Resources Council Annual Meeting, Sept. 25, Reno, Nev.

Mooney, W.D., Weaver, C.S., 1989. Regional crustal structure and tectonics of the Pacific Coastal States; California, Oregon, and Washington. In: Pakiser, L.C., Mooney, W.D. (Eds.), Geophysical Framework of the Continental United States: Boulder, Colorado, Mem. Geol. Soc. Amer., vol. 172, pp. 129–161.

Okaya, D., Henrys, S., Stern, T., 2002. Super-gathers across the South Island of New Zealand: double-sided onshore–offshore seismic imaging of a plate boundary. Tectonophysics 355, 247–263.

Ozalaybey, S., Savage, M.K., Sheehan, A.F., Louie, J.N., Brune, J.N., 1997. Shear-wave velocity structure in the northern Basin and Range province from the combined analysis of receiver functions and surface waves. Bull. Seismol. Soc. Am. 87, 183–199.

Pakiser, L.C., Brune, J.N., 1980. Seismic models of the root of the Sierra Nevada. Science 210, 1088–1094.

Pancha, A., Louie, J., Anderson, J.G., 2002. Reno area basin seismic response: ground motion simulation in Reno, Nevada. EOS Trans. Am. Geophys. Union 83 (Suppl. 47), F1055. (19 Nov.).

Phillips, D., 1990. Three-dimensional P and S velocity structure in the Coalinga region, California. J. Geophys. Res. 95, 15343–15364.

Podvin, P., Lecompte, I., 1991. Finite difference computation of traveltimes in very contrasted velocity models: a massively parallel approach and its associated tools. Geophys. J. Int. 105, 271–284.

Pullammanappallil, S.K., Louie, J.N., 1994. A generalized simulated-annealing optimization for inversion of first-arrival times. Bull. Seismol. Soc. Am. 84, 1397–1409.

Qin, F., Luo, Y., Olsen, K.B., Cai, W., Schuster, G.T., 1992. Finite-difference solution of the eikonal equation along expanding wavefronts. Geophysics 57, 478–487.

Roecker, S., 1982. Velocity structure of the Pamir—Hindu Kush region: possible evidence of subducted crust. J. Geophys. Res. 87, 945–960.

Ruppert, S., Fliedner, M.M., Zandt, G., 1998. Thin crust and active upper mantle beneath the Southern Sierra Nevada in the Western United States. Tectonophysics 286, 237–252.

Spieth, M.A., Hill, D.P., Geller, R.J., 1981. Crustal structure in the northwestern foothills of the Sierra Nevada from seismic refraction experiments. Bull. Seismol. Soc. Am. 71, 1075–1087.

Stewart, J.H., 1988. Tectonics of the Walker Lane belt western Great Basin—Mesozoic and Cenozoic deformation in a zone of shear. In: Ernst, W.G. (Ed.), Metamorphism and Crustal Evolution of the Western United States. Prentice-Hall, Englewood Cliffs, NJ, pp. 683–713.

Stewart, J.H., Carlson, J.E., 1977. Million-Scale Geologic Map of Nevada, vol. 57. Nevada Bureau of Mines and Geology Map, Reno, NV.

Thelen, Weston A., Smith, Shane B., Louie, John N., Concha-Dimas, Aline, 2002. Developing a geothermal indicator index from crustal geophysical data for the western Great Basin. EOS Trans. Am. Geophys. Union 83 (Suppl. 47), F1241. (19 Nov.).

Thompson, G.A., Catchings, R., Goodwin, E., Holbrook, S., Jarchow, C., McCarthy, J., Mann, C., Okaya, D., 1990. Geophysics of the western Basin and Range Province. In: Pakiser, L.C., Mooney, W.D. (Eds.), Geophysical Framework of the Continental United States, Am. Geophys. Union, pp. 177–204.

Um, J., Thurber, C.H., 1987. A fast algorithm for two-point seismic ray tracing. Bull. Seismol. Soc. Am. 70, 972–986.

Vidale, J.E., 1988. Finite-difference calculation of travel times. Bull. Seismol. Soc. Am. 78, 2062–2076.

Vidale, J.E., Helmberger, D.V., Clayton, R.W., 1985. Finite-difference seismograms for SH waves. Bull. Seismol. Soc. Am. 75, 1765–1782.

Wernicke, B., Clayton, R., Ducea, M., Jones, C.H., Park, S., Ruppert, S., Saleeby, J., Snow, J.K., Squires, L., Fliedner, M., Jiracek, G., Keller, R., Klemperer, S., Luetgert, J., Malin, P., Miller, K., Mooney, W., Oliver, H., Phinney, R., 1996. Origin of high mountains in the continents: the southern Sierra Nevada. Science 271, 190–193.

Wessel, P., Smith, W.H.F., 1991. Free software helps map and display data. EOS Trans. Am. Geophys. Union 72, 441.

Zelt, C., Ellis, M., 1989. Seismic structure of the crust and upper mantle in the Peace River Arch region, Canada. J. Geophys. Res. 94, 5644–5729.